Journal of the Korean Nuclear Society
Volume 19, Number 2, June, 1987

Effect of Preoxidation on the Zircaloy-4 Oxidation Behavior in a Steam and Water Mixture between 700°C and 850°C

Jong-Sung Yoo and In-Sup Kim
Korea Advanced Institute of Science and Technology
(Received April 3, 1987)

수증기와 물의 혼합 분위기에서 기산화층이 지르칼로이-4의 산화 거동에 미치는 영향

유 종 성·김 인 섭
한국과학기술원
(1987. 4. 3 접수)

Abstract

Experiments and numerical analysis have been performed to investigate the effect of preoxidation by oxidizing Zircaloy-4 specimens at a higher temperature after a period of exposure at a lower temperature. The oxidation experiments were performed between 700°C and 850°C after preoxidation at 650°C in a steam and water mixture for 600 seconds and 1,800 seconds. As the thickness of preoxidized layer increased, the oxidation rate of preoxidized specimens at higher temperature became lower than that of as-received claddings. A transition region of oxidation rate exist in the preoxidized specimens, and the region disappeared rapidly as the oxidation temperature increased. This effect appeared more clearly at lower temperatures. According to the results of numerical analysis performed in this study, the growth rate of oxide layer thickness and weight gains were similarly affected by the thickness of preoxidized layer.

요 약

핵연료 피복재(Zircaloy-4)에 생기는 얇은 산화층의 두께에 따른 고온에서의 산화 거동을 관찰하기 위하여 실험과 수치 계산을 수행하였다. 산화 실험은 수증기와 물의 혼합 분위기에서 지르칼로이-4판재 시편을 650°C에서 600초, 1,800초 동안 산화시켜서 산화층을 형성시킨 후 700°C와 850°C 사이의 온도에서 산화 거동을 관찰하였다. 기산화층의 두께가 두꺼울수록 고온에서의 산화율은 as-received cladding의 경우보다 낮았다. 기산화층이 형성된 시편에서는 산화율 천이 영역이 나타났으며 이 영역은 산화 온도가 올라감에 따라 점차로 소멸되었다. 기산화층의 영향은 낮은 온도(700°C)에서 가장 뚜렷하게 나타났다. 수치 계산 결과에 의하면, 산화층 증가율과 무게 증가는 실험 결과와 비슷하게 기산화층의 두께에 영향을 받았다.

I. Introduction

The zirconium-base alloys are widely used as cladding materials for the fuel element of nuclear power plants. These materials have high mechanical strengths, ductility and good corrosion resistance under normal operating conditions.[1,2]

In an accident like LOCA (Loss Of Coolant Accident), Zircaloy-4 tubes react with steam and are rapidly oxidized as the cladding temperature increases.[3,4] When they are oxidized, the yield strength of the Zircaloy-4 increases to some extent at first and immediately drops afterwards.[5,6] Due to oxygen intake, embrittlement of the cladding occurs.[7~9]

Several investigators[10~13] have reported that there are much differences in the oxidation behavior according to the period of oxidation when the claddings are oxidized in its fuel cycle. While the tubes are corroded very slowly in the operating temperature range, the higher temperature oxidation kinetics are affected by the presence of oxides formed during normal operations.

In this study, the effect of preoxidation was investigated to elucidate a possible mechanism for reduction in oxidation rate when the cladding material was oxidized at higher temperatures after preoxidizing at a lower temperature.

II. Mathematical Modeling

The equations describing the oxygen diffusiion in a system of oxide and α-Zircaloy (Fig. 1) are[14~16]

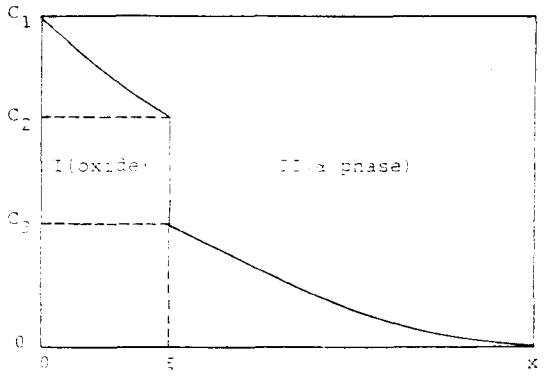

Fig. 1. Schematic Diagram of an Oxgen Concentration Profile in a System with Two Solid Phases I and II, and a Moving Interface at ξ. C_1 is the Equilibrium Concentration in Phase I in Contact with the Gas; C_2 in Phase I in Contact with Phase II: C_3 in Phase II in Contact with Phase I.

$$D_{\mathrm{I}}\frac{\partial^2 C_{\mathrm{I}}}{\partial X^2}=\frac{\partial C_{\mathrm{I}}}{\partial t},\quad D_{\mathrm{II}}\frac{\partial^2 C_{\mathrm{II}}}{\partial X^2}=\frac{\partial C_{\mathrm{II}}}{\partial t} \qquad (1)$$

where D_{I} and D_{II} are the diffusion coefficients of oxygen in the oxide(I) and the α phase (II), C_{I} and C_{II} are the oxygen concentrations in the oxide and the α phase, respectively.

A finite difference method with an implicit scheme was used to analyze the diffusion phenomena under the moving interface conditions. Applying a forward difference scheme, the implicit finite difference equations for the equation (1) can be expressed as follows

$$-RC_{j-1}^{k+1}+(1+2R)C_j^{k+1}-RC_{j+1}^{k+1}=C_j^k \qquad (2)$$

where $R=D\Delta t/\Delta x^2$, D is the diffusion coefficient (cm^2/s), j corresponds to the space variable and k to the time variable. Upon expanding the equation (2) in a matrix form, this reduces to two tridiagonal linear simultaneous equations as follows:

$$\begin{pmatrix} 1+2R_1 & -R_1 & 0 & \cdots & 0 & 0 \\ -R_1 & 1+2R_1 & -R_1 & \cdots & 0 & 0 \\ \cdots & \cdots & \cdots & \cdots & \cdots & \cdots \\ \cdots & \cdots & \cdots & \cdots & 1+2R_1 & -R_1 \\ 0 & 0 & 0 & \cdots & -\frac{2R_1}{2+p} & 1+\frac{2R_1}{1+p} \end{pmatrix} \begin{pmatrix} C(1) \\ C(2) \\ \cdots \\ C(M-2) \\ C(M-1) \end{pmatrix}^{(k+1)}$$

$$= \begin{pmatrix} C(1)+R_1C_1 \\ C(2) \\ \cdots \\ C(M-2) \\ C(M-1)+\dfrac{2R_1C_2}{(1+p)(2+p)} \end{pmatrix}^{(k)}, \quad \text{where } R_1=\frac{D_I\Delta t}{\Delta X^2} \tag{3}$$

$$\begin{pmatrix} 1+\dfrac{2R^2}{2-p} & -\dfrac{2R_2}{3-p} & 0 & \cdots & 0 & 0 \\ -R_2 & 1+2R_2 & -R_2 & \cdots & 0 & 0 \\ \cdots & \cdots & \cdots & \cdots & \cdots & \cdots \\ 0 & 0 & 0 & \cdots & -R_2 & 1+2R_2 \end{pmatrix} \begin{pmatrix} C(M+2) \\ C(M+3) \\ \cdots \\ C(N-1) \end{pmatrix}^{(k+1)}$$

$$= \begin{pmatrix} C(M+2)+\dfrac{2R_2C_3}{(2-p)(3-p)} \\ C(M+3) \\ \cdots \\ C(N-1)+R_2C_4 \end{pmatrix}^{(k)}, \quad R_2=\frac{D_{II}\Delta t}{\Delta X^2} \tag{4}$$

where p is the position when the interface is located between $M\Delta x$ and $(M+1)\Delta x$, and C_4 is a small fraction of C_3. M is the number of intervals of amplitude Δx in phase I and $(N-M)$ is its number in phase II. When n equals to $(M-1)$ and $(M+2)$, the corresponding equations are derived using the second-order Lagrange interpolation technique.

If at a given instant the interface coincides with a node, then $p=0$. As the interface moves ahead, p may exceed 1, then M is increased by 1 and p takes again the value between 0 and 1. In the two-phase system, when the interface does not coincide with the mesh point, oxygen concentrations near the interface can not be found directly. In these cases, the interpolation technique for calculating $C(M)$ and $C(M+1)$ at $(k+1)$-step is needed.[16]

To treat the effect of preoxidation between 700°C and 850°C, the oxygen concentrations at 650°C after 600 second and 1,800 second oxidation are used as input data for the calculation of the oxygen concentrations at the higher temperatures.

III. Experimental Procedure

The reactor-grade Sandvik Zircaloy-4 plates were used in this experiment. Specimens were weighed with use of the analytical microbalance with a precision of 0.1mg before they were oxidized in a tube furnace. Specimens were cleansed using petroleum ether and dried out to remove moisture before oxidized in a tube furnace.

In the case of oxidation of as-received claddings, the specimens were oxidized isothermally between 700°C and 850°C in the atmosphere of a steam and water mixture. Temperature control was carried out by a proportional type digital temperature controller and temperature variation of each specimen was found within the range of ±5°C by the thermocouple (type-K) located near the specimen in the tube furnace.

To form the preoxidized layer, the as-received claddings were oxidized in a steam and water mixture for 600 seconds and 1.800 seconds at 650°C. Each preoxidized specimen was reoxidized isothermally at a temperature between 700°C and 850°C to study the preoxidation effect.

Changes in specimen weight were measured

to check the oxidation rate. To measure the preoxidized layer thicknesses, the oxidized specimens were observed under an optical microscope.

IV. Results and Discussion

A. Analysis of Weight Gains

The thicknesses of preoxidized layer at 650°C were found to be 4μm after 600 second oxidation and 7μm after 1800 seconds. Figure 2 illustrates the data for the wegight gains per unit area of as-received specimens at each temperature. This shows the parabolic oxidation behavior. From the figures 3 through 6, the differences in weight gains between the preoxidized specimens and the as-received specimens are observed, and these differences are more pronounced in the preoxidized specimens with oxide layer of 7μm thickness.

The parabolic rate constant K_p in case of oxidation experiments of as-received claddings and the oxygen diffusion coefficients D_{ox}, D_α in the oxide and the phase, respectively, were found to be

$$K_p = 1.80 \times 10^4 \exp(-32700 \pm 500/RT) \quad (\mathrm{mg/cm^2})^2/\mathrm{sec}$$

$$D_{ox} = 0.04 \exp(-29508/RT) \quad (17) \quad \mathrm{cm^2/sec}$$

$$D_\alpha = 1.00 \exp(-49000/RT) \quad (16) \quad \mathrm{cm^2/sec}$$

where R is the gas constant (=1.9872cal/mole/K) and T is the absolute temperature(°K).

At first, the oxidation rate of the preoxidized specimens at a high temperature follows that of 650°C. But, as further oxidation take places, its oxidation rate changes to that of a high temperature which is different from the oxidation rate of as-received specimens.

It appeares that the transition region of oxidation rate exists in the preoxidized specimens and the transition region is more evident for the specimens oxidized at 700°C and 750°C than for those oxidized at 800°C and 850°C. The transition region disappears rapidly as the oxidation temperature increases. Before the transition

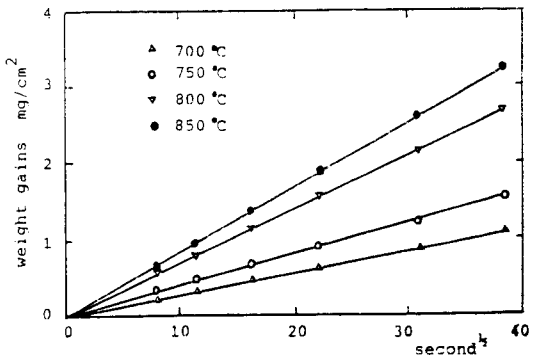

Fig. 2. Weight Gains Against $\sqrt{t}$ for Various Temperatures in a Steam and Water Mixture (as-received cladding)

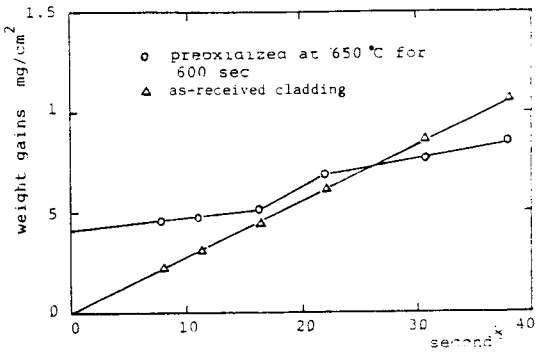

Fig. 3. Comparison of Weight Gains in Preoxidized Specimens with New Specimens at 700°C

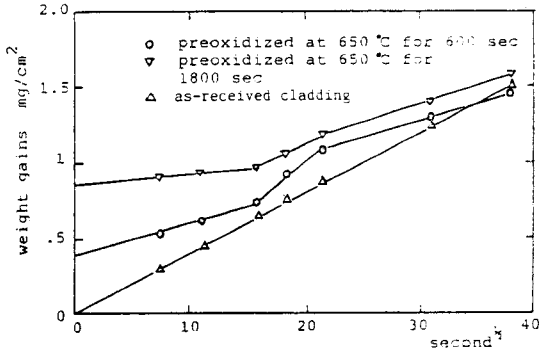

Fig. 4. Comparison of Weight Gains in Preoxidized Specimens with New Specimens at 750°C

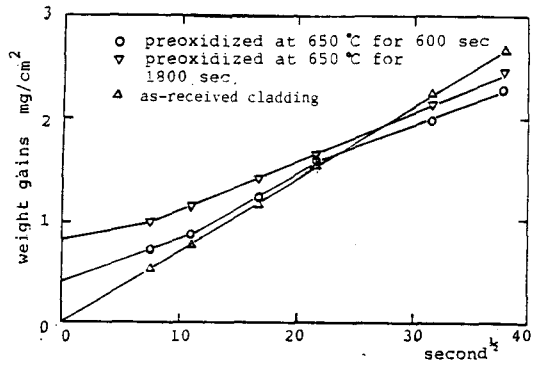

Fig. 5. Comparison of Weight Gains in Preoxidized Specimens with New Specimens at 800°C

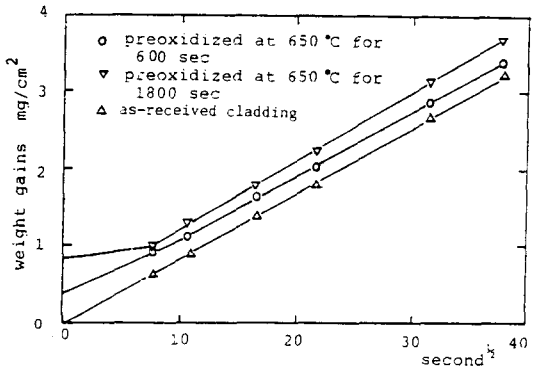

Fig. 6. Comparison of Weight Gains in Preoxidized Specimens with New Specimens at 850°C

at 850°C (Fig. 6), the weight gains increase more slowly for the preoxidized specimens with 7μm thick oxide layer than for those with 4μm thick oxide layer. After the transition, both weight gains increase at the same rate. At this temperature, the effect of preoxidation does not influence significantly the oxidation rate after the transition because of the fast oxygen diffusivity in Zircaloy-4 at high temperatures.[10]

B. Analysis of Numerical Results

Based on the numerical analysis introduced in section II, the thicknesses of oxide layer calculated by numerical method after considering the preoxidation effect are plotted as a function of square root of time in the figures 7 through 10.

Table 1. Parabolic Rate Constant and Interface Displacement Velocities in the As-received Claddings During 1500 Second Oxidation

T(°C)	K_p(mg/cm²)²/sec	v(cm/sec)
700	7.56×10^{-4}	5.586×10^{-7}
750	1.46×10^{-3}	8.241×10^{-7}
800	5.03×10^{-3}	1.151×10^{-6}
850	7.53×10^{-3}	1.540×10^{-6}

These figures show that there also exists the effect of preoxidation, and this effect is more pronounced with the increasing thickness of preoxidized layer. As oxidation temperature rises, effect of preoxidation becomes weaker because of the faster oxygen diffusivity at high temperatures.

The average values of the interface displacement velocity in the as-received claddings are given in Table 1 and at one temperature this velocity decreases as oxidation time increases due to oxygen saturation in the alpha phase.[16]

Since the interface displacement velocity is very sensitive to the gradient of oxygen concen-

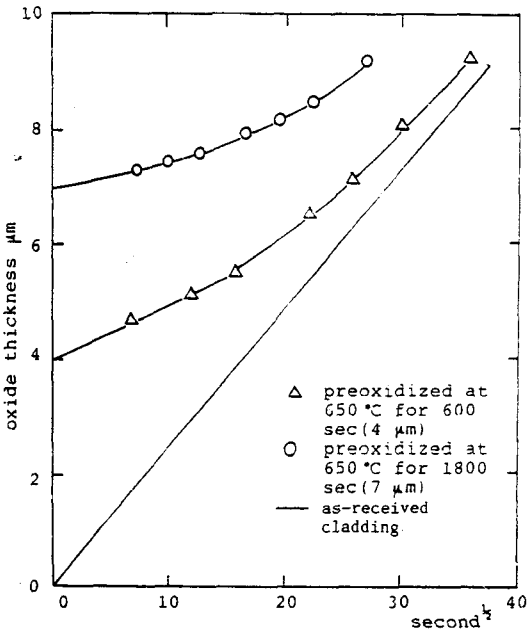

Fig. 7. Growth of Oxide Layer in Preoxidized Zircaloy-4 at 700°C from Numerical Analysis

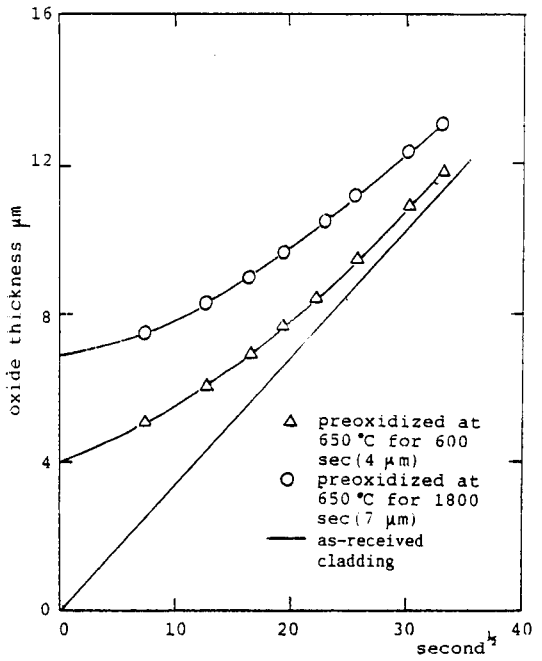

Fig. 8. Growth of Oxide Layer in Preoxidized Zircaloy-4 at 750°C

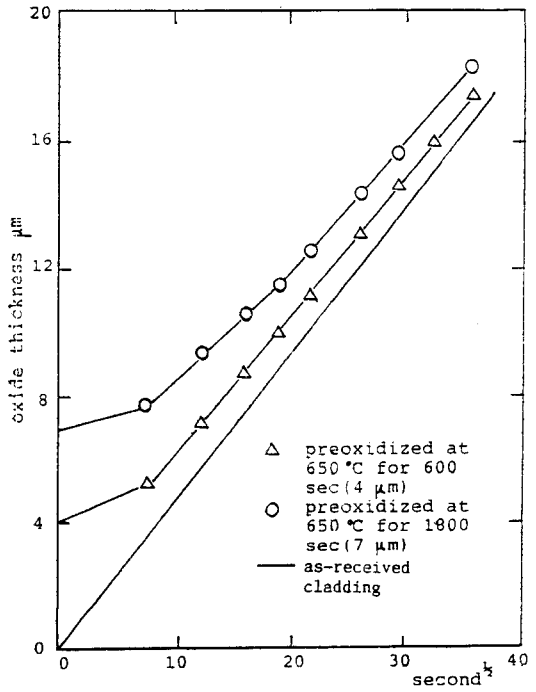

Fig. 9. Growth of Oxide Layer in Preoxidized Zircaloy-4 at 800°C

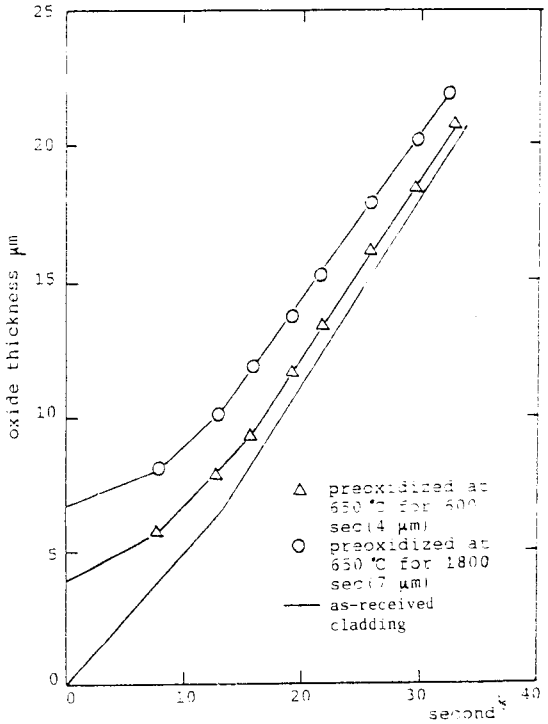

Fig. 10. Growth of Oxide Layer in Preoxidized Zircaloy-4 at 850°C

trations near the interface, the numerical values of the derivatives should be computed carefully. The Lagrange interpolation method with second-order polynomial applied to this problems is not proper because it fails to give the derivatives at the interpolated points.[15] The linear interpolation method to find the derivatives at the interface, however, is satisfactory, whereas the new oxygen concentrations near the interface were computed by second-order Lagrange interpolation method.

C. Discussions on Preoxidation Effect

The oxidized specimens were black, probably indicating an oxygen deficiency in the oxide layer.[18] B. Cox has considered that the black oxide film is due to the growth of the vacancy gradient.[19]

Analysis of the oxide film has shown that its chemical composition may differ from the stoichiometric proportions. It was reported[20] that the black protective oxide film shows an oxygen

deficiency, while the white friable oxide film has a chemical composition corresponding exactly to the formula ZrO_2.

The zirconium-dioxide belongs to the fluorite (CaF_2) structure with a lattice parameter of 5.272Å, which shows gross non-stoichiometry.[21]

In case of oxygen-deficient oxides, as in ZrO_{2-x}, diffusion rate can be expressed as follows[22]:

$$\text{Rate} \propto \exp(-\Delta G^0_{v_0}/RT) \quad (5)$$

where

$$-\frac{\Delta G^0_{v_0}}{RT}=\frac{1}{RT}\left[\frac{1}{2}\Delta\bar{H}_{O_2}-\frac{T}{2}(\Delta\bar{S}_{O_2}-6R\ln X+2R\ln 2)\right]$$

$\Delta G^0_{v_0}$=relative partial free energy accompanying the introduction of vacancy formation

$\Delta\bar{H}_{O_2}$=relative partial enthalpy of oxygen

$\Delta\bar{S}_{O_2}$=relative partial entropy of oxygen

x=a parameter showing the deviation from the stoichiometry of zirconium dioxide(ZrO_2)

Then the diffusion rate dependent upon the stoichiometry of the oxide is

$$\text{Rate}=R_0\exp(\Delta\bar{H}_{O_2}/RT)\exp\left[-\frac{1}{2R}(\bar{S}_{O_2}-6R\ln X+2R\ln 2)\right]=R_0'x^3 \quad (6)$$

where

$$R_0'=R_0\exp(\Delta\bar{H}_{O_2}/RT)\exp\left[-\frac{1}{2R}(\Delta\bar{S}_{O_2}+2R\ln 2)\right]$$

R_0=a parameter dependent upon the migration energy

From examining these relationships, it is clear that the more the oxide structure becomes defective, the easier the oxygen diffusion in metals takes place. This suggests the strong dependence of a diffusion coefficient upon the stoichiometry of the oxide.

Oxygen diffusion in Zircaloy-4 takes place through the anion vacancy in the oxide phase. The anion vacancy concentration is lower at 650°C (means low value of x) than at higher temperature, thus it takes a time for the anion defect structure at 650°C to equilibrate to that structure stable at higher temperatures.

As a consequence, when the claddings preoxidized at 650°C are oxidized at higher temperatures, the oxidation rate is lower than the one observed in the as-received claddings and a transition region of oxidation rate exists.

V. Conclusion

By experimental and numerical methods, it was confirmed that the preoxidation affects subsequent oxidation rate at higher temperatures and growth rate of oxide layer was influenced by the thickness of preoxidized layer. From these facts, it may be concluded that the preoxidized claddings show lower oxidation rate during exposure in high temperature steam and water mixture after transfering from low temperature, and a transition region of oxidation rate exist in the preoxidized claddings. This effect of preoxidation increased as the thickness of preoxidized layer increased and appeared more clearly at lower oxidation temperatures.

The parabolic rate constant K_p in case of as-received claddings between 700°C and 850°C was found to be

$$K_p=1.80\times10^4\exp(-32700\pm500/RT)\ (\text{mg/cm}^2)^2/\text{sec}$$

The mechanism of this preoxidation effect was explained by the defect structure of oxygen-deficient oxides although more experimental and microstructural analysis are required to verify this mechanism.

References

1. J.T. Adrian Roberts, "Structural Materials in Nuclear Power Systems," Plenum Press, New

York, 1981.
2. Benjamin M. Ma, "Nuclear Reactor Materials and Applications," Van Nostrand Reinhold Co., New York, 1983.
3. L. Baker and L.C. Just, "Studies of Metal-Water Reactions at High Temperatures," ANL-6548, May, 1962.
4. R.E.Pawel, J.V. Cathcart and J.J. Campbell, J. Nucl. Mat. 82(1979) 129-139.
5. R.H. Meservey and R. Herzel, USAEC IN-1389, Idaho Nuclear Co., 1970.
6. L.R. Bunnel, J.N. Bates and G.B. Mellinger, J. Nucl. Mat. 116(1963) 219-232.
7. H.M. Chung and T.F. Kassner, "Embrittlement Criteria for Zircaloy Fuel Cladding Applicable to Accident Situations in Light-Water Reactors," NUREG/CR-1344, ANL-79-48.
8. A.S. Rizkalla, R.A. Holt and J.J. Jonas, "Effect of Oxygen on the Deformation of Zircaloy-2 at Elevated Temperature", Zirconium in the Nuclear Industry (Fourth Conference) ASTM STP 681, 1979, pp. 497-513.
9. D.O. Hobson and P.L. Rittenhouse, "Embrittlement of Zircaloy-Clad Fuel Rods by Steam During LOCA Transients," ORNL-4758, Jan. 1972.
10. R.R. Biederman, R.D. Sisson, J.K Jones and W.G. Dobson, "A Study of Zircaloy-4 Steam Oxidation Reaction Kinetics," EPRI NP-734, pt. 2, 1978.
11. M.F. Sheppard and C. Tyzack, "Corrosion Monitoring of Steam Generating Heavy Water Reactor Pressure Tubes," Zirconium in the Nuclear Industry, ASTM STP 633, 1977, pp. 258-280.
12. D.E. Thomas and S. Kass, J. Electrochem. Soc. 104(1957) 261.
13. S. Kass, "Corrosion of Prefilmed Zircaloy," Corrosion 23(1967) 374.
14. W. Jost, "Diffusion in Solids, Liquids, and Gases," Academic Press, N.Y., 1960.
15. E.A. Garcia, J. Nucl. Mat. 92(1980) 249-256.
16. A. Denis and E.A. Garcia, J. Nucl. Mat. 114 (1983) 75-84.
17. W.G. Dobson and R.R. Biederman, "ZORO 1-A Finite Difference Computer Model for Zircaloy-4 Oxidation in Steam," EPRI NP-347, Dec. 1976.
18. S. Aronson, J. Electrochem. Soc. 108(1961) 312.
19. B. Cox, Corrosion, 16(1960) 380.
20. B.G. Parfenov, V.V. Gerasimov and G.I. Venediktova, "Corrosion of Zirconium and Zirconium Alloys," IPST Cat. No. 5403, Jerusaleum, 1969 (Translated From. Lussian, Atomizdat Moskva 1967).
21. D.K. Smith and C.F. Cline, J. Am. Ceram. 45 (1962) 249.
22. O. Toft Sorensen, "Nonstoichiometric Oxides," Academic Press, New York, 1981.